MIRI DFM 289 – 04.02

Mid Infra-Red Instrument (MIRI)

Predicted QE of the MIRI Flight Detectors

13 February 2009

M. Ressler
MIRI Project Scientist, JPL

Jet Propulsion Laboratory
California Institute of Technology

Predicted QE of the MIRI Flight Detectors

Mike Ressler
JPL MIRI Project Scientist

February 13, 2009

1 Overview

Because it is not possible to measure the spectral quantum efficiency (QE; more appropriately the quantum yield, but we assume that the detectors will always be operated with a gain of 1, thus they are equivalent) of the anti-reflection (AR) coated MIRI detector arrays directly using Fourier Transform Spectrometers, we use a multistep process to predict the QE of the flight detectors. The effective QE is the product of the efficiency of the detector layers ability to absorb photons and the reflection losses from the front surface of the detector layers, so the challenge is to accurately estimate these two quantities as a function of wavelength.

To get at the aborption efficiency, it is possible to measure the spectral QE of uncoated test structures that are included on the detector wafers. In this case, the front-surface reflection loss is essentially constant (the index of refraction of silicon is an essentially constant 3.42 over the 5 to 28 micron wavelength range) and can be predicted, thus the measurements yield a reliable value of the internal QE. This is normally performed on 2 to 4 diodes per wafer and the mean of these can be taken to be the raw or uncoated QE for each of the detector die.

The reflectance of the AR coatings can be measured by depositing a layer of coating material on a silicon wafer of thicknesses matching those used on the detectors. It is important to have a sufficient surface roughness for these measurements, and in the measured data, the predicted reflectance begins to deviate from the measurements at around 16 microns due to this effect.

2 Reflectance

The reflectance data are given in Figures 1 and 2. The blue curves are the measured data, while the dashed red curves are the fitted predictions assuming the coating is a quarter-wave, single-layer coating of ZnS with an index of refraction of 2.05 (also constant over wavelength). The "6 μm" coating uses a layer thickness of 0.72 μm, while the "16 μm" coating uses a 2.08 μm thick coating. The fit is remarkable for a very simple model (e.g. no contaminants, oxidation, etc.) with the exception of the long wavelength surface roughness deficiency that becomes significant for wavelengths > 16 μm. For the corrections to the detector QE, I assume that the models provide an adequate prediction of the surface reflection and use them in preference to the measured data.

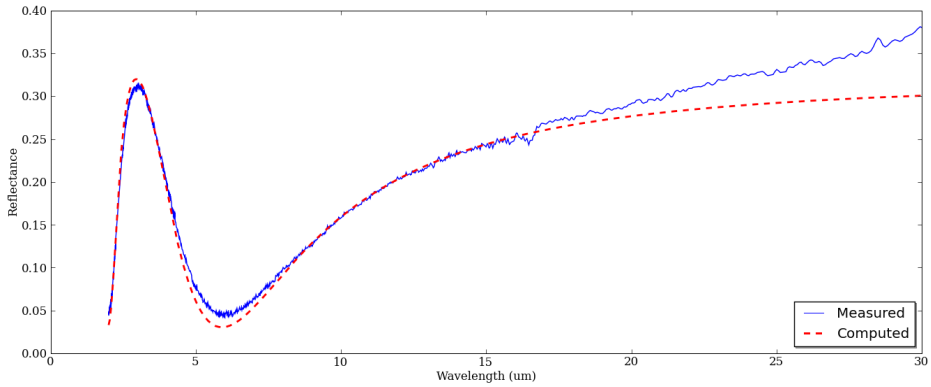

Figure 1: The reflectance of the 6 μm AR coating.

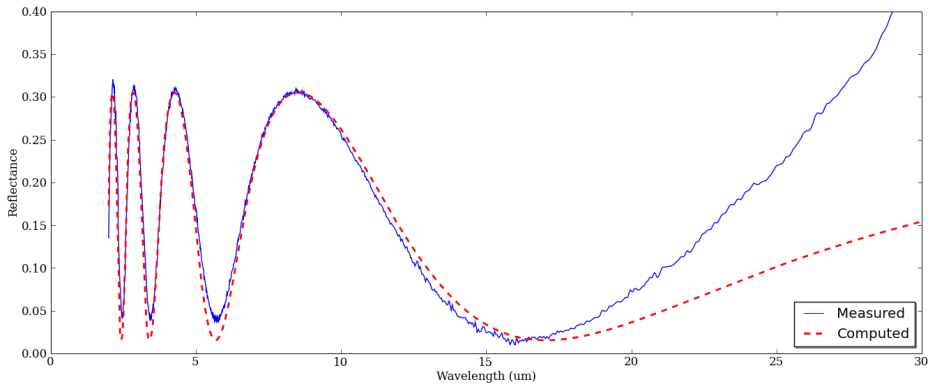

Figure 2: The reflectance of the 16 μm AR coating.

3 Test Diode QE Measurements

Included on every detector wafer are a number of test structures in addition to the actual detector die. Each of these structures as several photodiodes of varying sizes, and these can be used to judge the quality of that particular wafer. MIRI developed two types of wafer: a "baseline" detector that used higher impurity doping and a thicker active layer, and a "contingency" detector that had a lower doping concentration and a thinner active layer. Figure 3 shows measured curves from 6 diodes from two different wafers using an FTS. They are sufficiently close in performance that I average them together and use that single curve to predict the performance for both the imager and long-wavelength (LW) spectrometer FPMs. The uncertainty associated with the measurement is given as the dashed line at the bottom of the plot. The random uncertainty is typically less than 2%, but the overall flux calibration error in absolute units is unknown. All curves from the FTS are normalized to the flux measured at 9 μm using a blackbody source and a filter. While it is believed that the uncertainty in this normalization is also on the order of a few percent, it has not been correlated to a NIST-traceable flux calibration.

Figure 4 shows similar data for a contingency wafer. Again, the four diodes measured on this wafer are very similar in character and have been average for the prediction of the short-wavelength

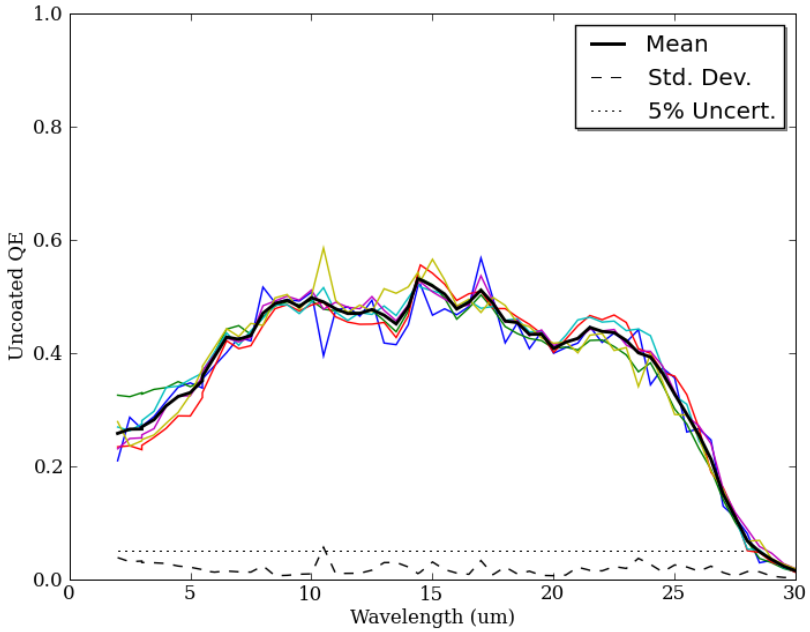

Figure 3: Measured QE of test diodes from "baseline" detector wafers. The mean value is given as a heavy black line.

(SW) spectrometer FPM.

4 Predicted FPM Performance

With these measurements in hand, we can predict the FPM performance by dividing the measured QEs by the known 69% transmission (1.0 – reflectance) of uncoated silicon, then multiplying by the predicted transmission of AR-coated silicon. Figures 5 through 7 show these predictions.

The QE requirement for the imager is relatively open ended: 50% for wavelengths < 19 μm, and 38% for wavelengths > 19 μm. The low resolution grism spectrometer, which shares this FPM, has a requirement of 38% from 5.5 to 9.5 μm. These requirements are met within the passbands of the filters actually used by MIRI with the exception of the 25.5 micron filter, where the naturally dropping QE goes below the requirement at about 25 μ. The MIRI sensitivity model shows that the FRD-level sensitivity requirements are still met in spite of this behavior, with the expense of reduced margin. This rolloff has been noted in every system and subsystem review since the FPM PDR, and has been accepted by the MIRI Science Team.

The SW FPM meets its requirements over the 5.5 to 12 μm range with a very minor deviation ($\sim$2%) at the short wavelength edge. This again has no impact on the FRD-level sensitivity.

The LW FPM is in the same position as the other two FPMS: it meets the requirement over most of the wavelength range (12 – 27 μm) with a couple of minor deviations until the response begins to drop dramatically at 24 μm. Again, this performance has been noted and accepted by the Science Team.

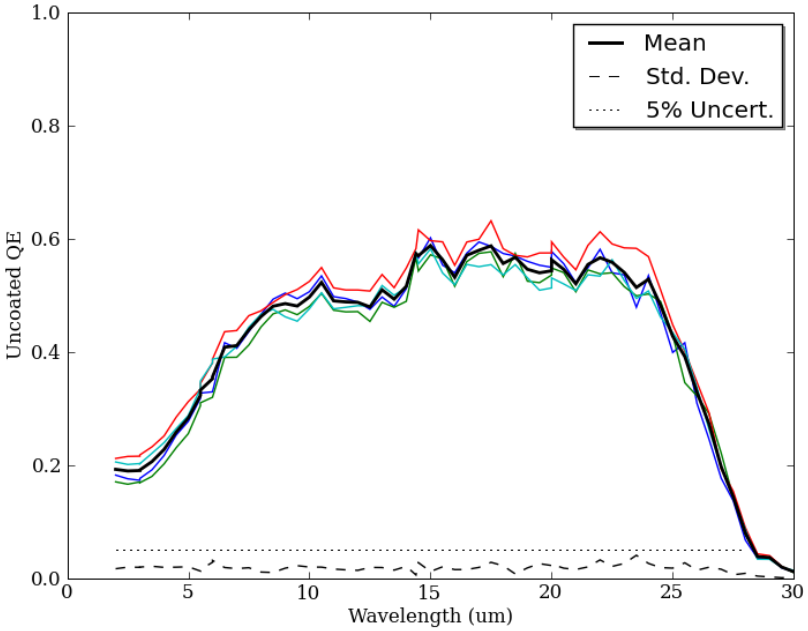

Figure 4: Measured QE of test diodes from a "contingency" detector wafer. The mean value is given as a heavy black line.

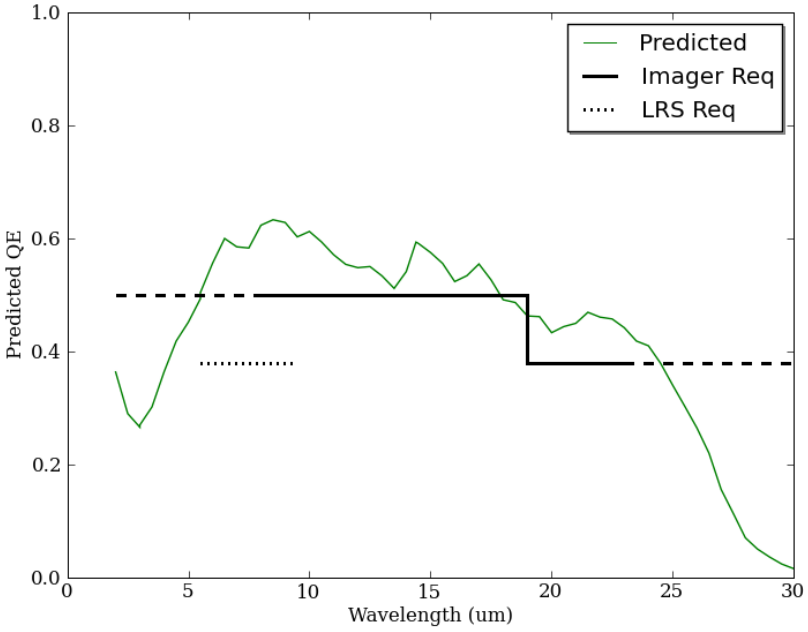

Figure 5: Predicted QE for the imager, FPM 106.

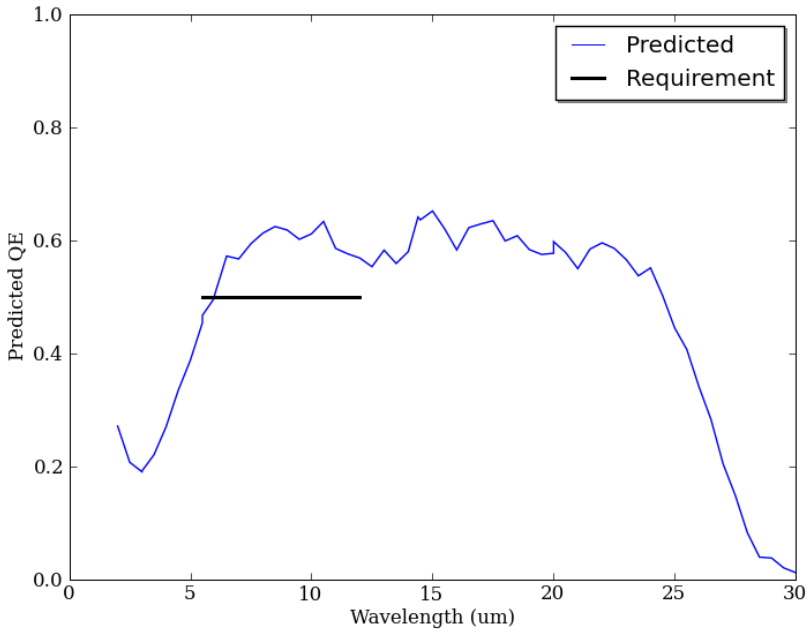

Figure 6: Predicted QE for the SW spectrometer, FPM 105.

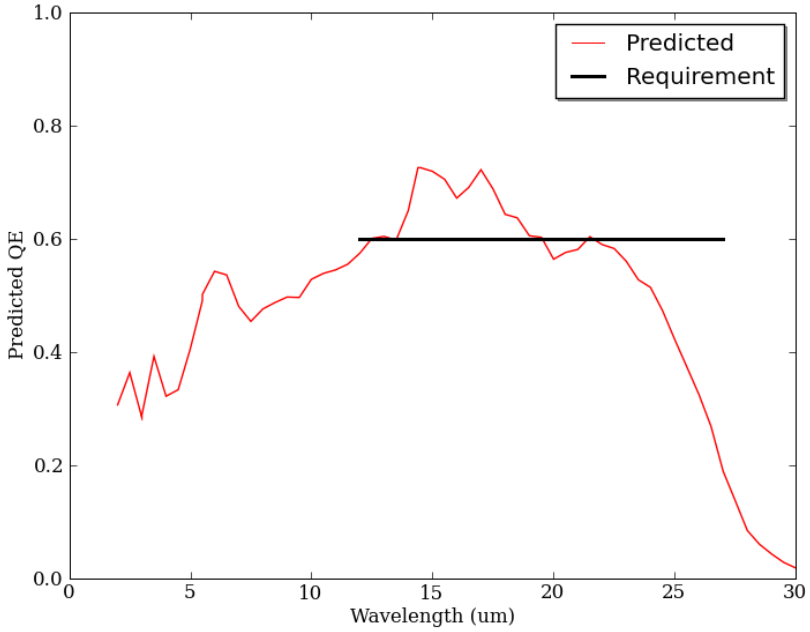

Figure 7: Predicted QE for the LW spectrometer, FPM 104.